

An Application of the Level Set Method to Underwater Acoustic Propagation

Sheri L. Martinelli^{1,2,*}

¹ *Torpedo Systems Department, Naval Undersea Warfare Center, 1176 Howell Street, Newport, Rhode Island 02841, USA.*

² *Division of Applied Mathematics, Brown University, Providence, Rhode Island 02912, USA.*

Received 19 March 2011; Accepted (in revised version) 23 December 2011

Communicated by Chi-Wang Shu

Available online 8 May 2012

Abstract. An algorithm for computing wavefronts, based on the high frequency approximation to the wave equation, is presented. This technique applies the level set method to underwater acoustic wavefront propagation in the time domain. The level set method allows for computation of the acoustic phase function using established numerical techniques to solve a first order transport equation to a desired order of accuracy. Traditional methods for solving the eikonal equation directly on a fixed grid limit one to only the first arrivals, so these approaches are not useful when multi-path propagation is present. Applying the level set model to the problem allows for the time domain computation of the phase function on a fixed grid, without having to restrict to first arrival times. The implementation presented has no restrictions on range dependence or direction of travel, and offers improved efficiency over solving the full wave equation which under the high frequency assumption requires a large number of grid points to resolve the highly oscillatory solutions. Boundary conditions are discussed, and an approach is suggested for producing good results in the presence of boundary reflections. An efficient method to compute the amplitude from the level set method solutions is also presented. Comparisons to analytical solutions are presented where available, and numerical results are validated by comparing results with exact solutions where available, a full wave equation solver, and with wavefronts extracted from ray tracing software.

AMS subject classifications: 65M06, 65M22, 65M25

PACS: 43.30.Gv, 43.30.Zk

Key words: Geometric acoustics, level set method, high-frequency acoustic propagation, WENO method.

*Corresponding author. *Email address:* sheri_martinelli@brown.edu (S. L. Martinelli)

1 Introduction

In this work, a fixed-grid model is applied to computational, high-frequency, underwater acoustic propagation. The proposed method builds upon the foundation established by Osher, Cheng, Kang, Shim, and Tsai [1] in which a level set method for geometric optics was introduced. High frequency propagation modeling in underwater acoustics is traditionally accomplished via ray tracing. Rather than solve for the acoustic pressure directly, the geometric optics approximation to the wave equation is employed to solve for a more slowly varying phase function and a separate amplitude function. Ray tracing solves the eikonal equation for the phase using the method of characteristics. When rays (characteristics) diverge, eventually they do not cover enough physical space, and well-resolved solutions are not available on any uniform grid.

Several computational approaches in addition to ray tracing already exist which can accurately solve the equations of acoustic propagation. However, these are not appropriate methods at high frequencies where required grid sizes become large enough to overwhelm computational resources. Ray tracing is therefore the current standard for high frequency or long range propagation modeling in underwater acoustics. The level set method may provide a practical alternative to ray tracing for solving the high frequency approximation to the wave equation for certain applications in which the need for control over solution accuracy is balanced against the need for computational speed. Such applications include modeling propagation in shallow water environments where multi-path propagation leads to combinatorial expense in the tabulation of returns from numerous eigenrays (one-way source to receiver paths). The effects of source and receiver beam patterns combined with the divergence of rays from the source often lead to poor reconstruction of the pressure field, especially in the presence of variable bathymetry or surface waves.

The difficulties with the Lagrangian approach are familiar from studies of long range acoustic propagation. The ray chaos problem was discussed in [2]. The term "ray chaos" generally refers to the phenomenon whereby small perturbations in the ray shooting angle result in large variations in the resulting trajectories. When chaotic rays are present, a high degree of precision is required to specify shooting angles in order to be able to locate eigenrays. In [3], Collins and Kuperman suggested an alternative method to compute eigenrays in the presence of ray chaos, i.e., the boundary value problem perspective vice an initial value problem (e.g., shooting method) for locating eigenrays, but their method relied on direct path optimization and did not allow for bottom or surface reflections. Godin [4] examined the behavior of rays versus that of wavefronts under weak sound speed fluctuations and showed that wavefronts are much more stable than rays, in the sense that the significant ray perturbations tend to occur along the wavefronts rather than across them. These results suggest that a propagation model based on acoustic wavefronts would be a useful tool for the underwater acoustics community.

The level set method is a wavefront-based model. By solving on a fixed grid in the phase space and evolving entire wavefronts in time, the eigenray (boundary-value) prob-

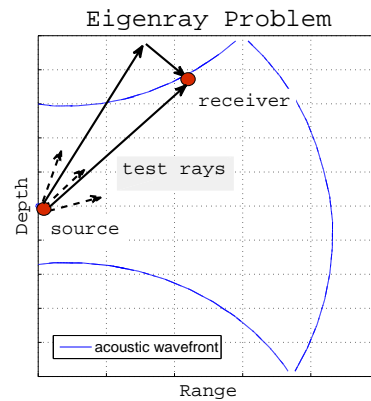


Figure 1: Arrivals at a given point in space are determined by wavefront crossing rather than shooting test rays.

lem is eliminated. Thus in complex domains, e.g., shallow water, even though the level set problem is posed in high dimensional phase space, improvement in computational speed may be observed because it would no longer be necessary to use a large number of test rays to determine a solution at a given point in space; this idea is illustrated in Fig. 1.

Level set methods are generic, computational techniques introduced by Osher and Sethian [5] for tracking the evolution of moving curves and surfaces. The advantage of this approach is that standard partial differential equation (PDE) solvers can be employed to solve the problem on uniform grids which may then be refined to reduce the global error. Level set methods achieve this by representing the propagating surface implicitly as the zero level set of a function in a higher dimensional space. This zero level set is then transported via the underlying velocity field. In the case of acoustic propagation in isotropic media, the propagation direction is normal to the propagating surface (wavefront). The extension to phase space allows for the computation of multi-valued solutions in the physical space. Multi-path propagation is handled naturally by ray tracing, but becomes an issue when solving on a fixed grid. In physical space, the multiply-valued solutions violate well-posedness of the problem. The bicharacteristic curves, an extension of the characteristics to the phase space, are single-valued however and hence working in the phase space, one can capture multi-path arrivals.

Eulerian (fixed grid) geometric optics has been an active research area in the scientific computing community for quite some time. Benamou [6] provides an overview of approaches to this problem. The most similar approach to the level set method is the segment projection method [7] in which wavefronts are tracked in phase space as projections onto each two dimensional subspace of the three dimensional phase space. This method is effective, but requires complicated bookkeeping in order to reconstruct wavefronts. The approach of Osher, et al. propagates the entire wavefront in the phase space where the bicharacteristics of the eikonal equation are well-behaved. In [8], Qian, et al. build upon [1] by extending the method to propagation in anisotropic materials. In [9], a method for incorporating reflecting boundaries is introduced. An alternative approach

to handling reflections is proposed in [10], although the results in this work are tied to assumptions on the domain geometry which do not extend easily to general scenarios in shallow water acoustics. Qian and Leung [11, 12] developed a level set method for the paraxial approximation. This approximation is commonly applied to ray tracing implementations as it reduces the number of independent equations to solve by propagating in a direction that increases monotonically with time (e.g., range). The approach of Qian and Leung reduces the dimensionality of the problem, but introduces an additional equation to be solved in the phase space to compute arrival times. This method addresses long range propagation problems, but the present work is primarily concerned with reflections and scattering back toward the source, which are precluded by the paraxial assumption.

The purpose of this work is to demonstrate an application of these foundations to the specific problem of high frequency underwater acoustics. A fast computational method for computing the amplitude due to spreading along a wavefront that is compatible with the framework of the level set method is also introduced for a more complete description of the acoustic pressure field. The proposed method is based on a ray approach to avoid extra computation in the higher-dimensional phase space, but takes advantage of the phase information provided by the level set method. Section 2 reviews background material and provides an overview of the method. Section 3 offers a description of the implementation, presenting the necessary components to implement a level set method for underwater acoustics, and in Section 4, some preliminary results demonstrating the algorithm's performance in a few sample cases including varying sound speed profiles and reflecting boundaries are presented. Results are summarized and section 5 concludes.

2 Background

2.1 High frequency acoustics and the eikonal equation for the phase

The high frequency wave equation results from application of a classical asymptotic approximation to the linear wave equation. Following [13], start with the d -dimensional linear wave equation for the acoustic pressure in a medium with constant density and variable sound speed function given by $c(\mathbf{x})$:

$$p_{tt} - c(\mathbf{x})^2 \Delta p = 0, \quad (2.1)$$

where $(t, \mathbf{x}) \in \mathbb{R}^+ \times \Omega$, $\Omega \subset \mathbb{R}^d$, and it is assumed that appropriate initial and boundary conditions are available. At very high frequencies (or more generally, when the wavelength is very small relative to the domain geometry), the solutions to this equation exhibit rapid oscillations. In order to be able to reasonably compute these solutions, apply the geometric optics approximation by assuming a solution of the form

$$p(t, \mathbf{x}) = e^{i\omega S(t, \mathbf{x})} \sum_{k=0}^{\infty} A_k(t, \mathbf{x}) (i\omega)^{-k}. \quad (2.2)$$

Upon substitution into the wave equation (2.1), this expression yields the eikonal equation for the phase function S from the highest order terms in ω

$$S(t, \mathbf{x}) \pm c |\nabla S(t, \mathbf{x})| = 0 \quad (2.3)$$

and a transport type equation for the first amplitude term

$$(A_0)_t + c(\mathbf{x}) \frac{\nabla S \cdot \nabla A_0}{|\nabla S|} + \frac{c(\mathbf{x})^2 \Delta S - S_{tt}}{2c(\mathbf{x}) |\nabla S|} A_0 = 0. \quad (2.4)$$

Similar transport equations can also be derived for the remaining amplitude terms, however for $\omega \gg 1$, only the two leading terms in the expansion are significant (this is the geometric optics approximation).

The weakly coupled system consisting of (2.3) along with (2.4) form the equations of high frequency acoustics.

2.2 Level set method for the eikonal equation

The eikonal equation is a Hamilton-Jacobi type equation with Hamiltonian given by $H(\mathbf{x}, \mathbf{k}) = c(\mathbf{x}) |\mathbf{k}|$. The vector-valued variable \mathbf{k} is associated with ∇S . First order PDE of this type can be solved locally via the method of characteristics by expressing (2.3), where, without loss of generality, only the equation with the plus sign (propagation outward from the initial wavefront) is considered, in terms of the phase space variables \mathbf{x} and \mathbf{k} . The Hamilton-Jacobi formulation is in the full phase space, where the variable \mathbf{k} is the generalized momentum. The characteristic equations are given by

$$\dot{\mathbf{x}}(t) = \nabla_{\mathbf{k}} H(\mathbf{x}, \mathbf{k}) = c(\mathbf{x}(t)) \frac{\mathbf{k}(t)}{|\mathbf{k}(t)|}, \quad (2.5a)$$

$$\dot{\mathbf{k}}(t) = -\nabla_{\mathbf{x}} H(\mathbf{x}, \mathbf{k}) = -|\mathbf{k}(t)| \nabla_{\mathbf{x}} c(\mathbf{x}(t)), \quad (2.5b)$$

with given consistent initial conditions $\mathbf{x}(0) = \mathbf{x}_0$, $\mathbf{k}(0) = \mathbf{k}_0 = \nabla_{\mathbf{x}} S(0, \mathbf{x}_0)$. Conservation of the Hamiltonian ensures that, for $H \equiv 1$,

$$|\mathbf{k}| = |\nabla S| = \frac{1}{c(\mathbf{x})} \quad (2.6)$$

holds.

The ray tracing approach involves computing $\mathbf{x}(t)$ from (2.5), typically using arclength parameterization rather than unscaled time. The difficulty with solving (2.3) on a fixed grid is that, in general, rays may cross, generating multi-valued solutions for the phase function S at some points. Thus standard PDE solvers fail in this case. One of the earlier methods for dealing with this situation was to compute the viscosity solution [14] which forces uniqueness by computing only the first arrival time. However, in applications, multi-valued arrival times are often desired. The level set method is able to handle

multi-valued arrival times by working in the phase space, where the bicharacteristics do not suffer from this problem [1].

In ray tracing, the ordinary differential equations (2.5) are solved along the ray from a starting point, \mathbf{x}_0 , on the initial wavefront. Often these equations are parameterized with respect to arclength in cylindrical coordinates in the presence of azimuthal symmetry, (r, z) , and the initial conditions are specified by a take-off angle. The level set method is based rather on an implicit representation of the wavefront. That is, the wavefront is not expressed explicitly as a function in the physical space, but is instead embedded as the zero level set of a function that is defined in a higher dimensional space (the phase space). Thus, a function that may be multi-valued or otherwise poorly behaved in the physical space is represented by a smoothly varying and well-defined quantity in the phase space. In fact, given the restriction (2.6), it is not necessary to utilize the full phase space in order to find S , since the magnitude $|\mathbf{k}|$ is fixed, the dimension can be reduced by one. For an example with two dimensional physical space, let

$$\mathbf{k} = \begin{pmatrix} |\mathbf{k}| \cos \theta \\ |\mathbf{k}| \sin \theta \end{pmatrix}, \quad (2.7)$$

then only θ need be considered an independent variable. In this representation, θ represents the propagation direction of the wavefront, and $\mathbf{k} = \left(\frac{\cos(\theta)}{c}, \frac{\sin(\theta)}{c} \right)$. So for two-dimensional physical space, the reduced phase space has three dimensions. It is desirable to work in the reduced phase space rather than full phase space for computational efficiency.

In two-dimensional propagation, since the wavefront is a curve in three-dimensional reduced phase space, define a vector-valued function

$$\Phi = \begin{pmatrix} \phi_1 \\ \phi_2 \end{pmatrix}, \quad (2.8)$$

referred to as the "level set function" [1] in the phase space. Define the two components, $\phi_1(t, \mathbf{x}, \mathbf{k})$ and $\phi_2(t, \mathbf{x}, \mathbf{k})$, such that the initial wavefront is embedded in the intersection of the zero level sets of ϕ_1 and ϕ_2 , i.e., the projection onto the physical space of the set $\{(\mathbf{x}, \mathbf{k}) | \phi_1(0, \mathbf{x}, \mathbf{k}) = \phi_2(0, \mathbf{x}, \mathbf{k}) = 0\}$. Fig. 2 offers an example of the implicit wavefront representation as the intersection of level set surfaces for two level set functions for a two-dimensional physical space.

To evolve the level set functions, note that the wavefront propagates in the direction of its normal, which is the local ray direction, given by $\frac{\mathbf{k}}{|\mathbf{k}|}$. Consider the zero level set of a component, ϕ_i , evaluated on the ray in phase space, i.e., $\phi_i(t, \mathbf{x}(t), \mathbf{k}(t)) = 0$. Differentiating in time and substituting from (2.5) shows that ϕ_i must satisfy the Liouville equation,

$$\frac{\partial \phi_i}{\partial t} + c(\mathbf{x}) \frac{\mathbf{k}}{|\mathbf{k}|} \cdot \nabla_{\mathbf{x}} \phi_i - |\mathbf{k}| \nabla_{\mathbf{x}} c(\mathbf{x}) \cdot \nabla_{\mathbf{k}} \phi_i = 0. \quad (2.9)$$

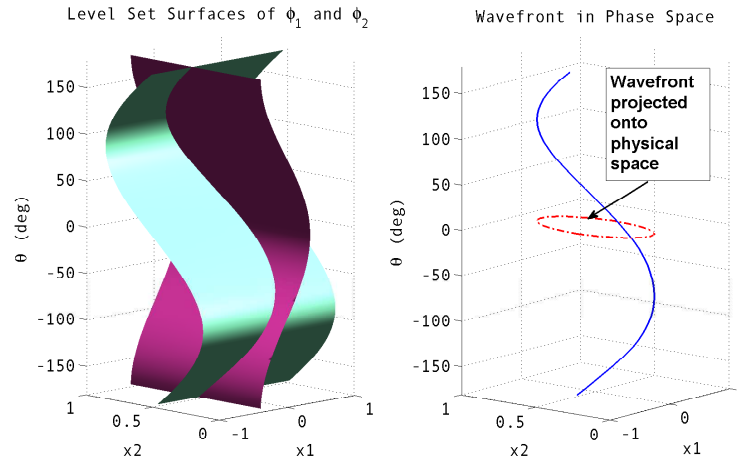


Figure 2: Implicit representation of 2D wavefront in the phase space.

In the reduced phase space for the two dimensional problem, (2.9) reduces to the following transport equation

$$\frac{\partial \phi_i}{\partial t} + \mathbf{V} \cdot \nabla \phi_i = 0, \quad i=1,2 \tag{2.10}$$

with the velocity field \mathbf{V} given as

$$\mathbf{V} = \begin{pmatrix} c(\mathbf{x}) \cos \theta \\ c(\mathbf{x}) \sin \theta \\ \frac{\partial c}{\partial x_1} \sin \theta - \frac{\partial c}{\partial x_2} \cos \theta \end{pmatrix}, \tag{2.11}$$

where $\mathbf{x} = (x_1, x_2)$ and θ is the direction of propagation in the x_1 - x_2 coordinate plane. This velocity field is derived directly from the ray equations (2.5). The functions ϕ_1 and ϕ_2 are defined at $t=0$ so that the known initial wavefront is embedded as the intersection of the zero level surfaces of the two functions. It is convenient if the source can be parameterized in θ so that it can be described as

$$\begin{aligned} x_1 &= f_1(\theta), \\ x_2 &= f_2(\theta). \end{aligned}$$

Then ϕ_1 and ϕ_2 can be initialized as

$$\phi_1(0, x_1, x_2, \theta) = x_1 - f_1(\theta), \tag{2.12a}$$

$$\phi_2(0, x_1, x_2, \theta) = x_2 - f_2(\theta). \tag{2.12b}$$

For instance, if the wavefront is a circle in the $x_1 x_2$ plane with radius α centered at some point (x_1^0, x_2^0) ,

$$\begin{aligned} \phi_1(0, x_1, x_2, \theta) &= x_1 - x_1^0 - \alpha \cos \theta, \\ \phi_2(0, x_1, x_2, \theta) &= x_2 - x_2^0 - \alpha \sin \theta \end{aligned}$$

defines such a choice. Letting $\alpha \rightarrow 0$ gives an appropriate initial condition for a point source at (x_1^0, x_2^0) . The two level set surfaces are orthogonal, an important property since recovering the wavefront involves seeking the intersection of the level set surfaces. Eq. (2.10) represents a decoupled hyperbolic system and can be evolved in time using appropriate numerical techniques. The wavefront, $W(x_1, x_2; t)$ may be recovered at any time t as

$$W(x_1, x_2; t) = \{(x_1, x_2) | \phi_1(t, x_1, x_2, \theta) = \phi_2(t, x_1, x_2, \theta) = 0\}. \quad (2.13)$$

A more thorough description of the level set method for geometric optics can be found in [1].

2.3 Amplitude

In underwater acoustics, it is important to be able to compute not only the arrival times of the wavefronts, but the amplitudes as well in order to properly simulate reverberation or scattering for simulation and testing purposes. The amplitude (alternately expressed as a transmission loss) consists primarily of three components: loss due to geometric spreading, scattering loss, and attenuation loss. Attenuation causes a plane wave to decay according to an exponential law $A = A(0)e^{-\alpha r}$ due to the conversion of acoustic energy into heat. Given information about an environment, this would be applied as a factor multiplying the other losses. To handle scattering loss (e.g., from surface, bottom, and objects in the environment), models have been developed for which the loss is specified as a function of incidence angle [15]. The angles of incidence and reflection at the boundary are readily available from the level set data, thus could be incorporated into the boundary conditions.

The greater difficulty is posed by the computation of the spreading loss. An important consideration here is computational speed. In situations where the loss is only required at a few distinct locations in space at a given time, loss data need not be computed everywhere on the wavefront. This can be exploited in order to speed up the algorithm. For other applications, accuracy may be more important than speed, in that case it may be desirable to have full wavefront information. Methods for computing the spreading loss along a ray have long been established, cf. [13, 16]. In [17–19], it is shown that the related quantity $\rho = \frac{A_0^2}{c^2}$ also satisfies (2.9). However this is a full phase space approach, which significantly increases the computational burden. The idea of the approach presented here is to combine the simplicity of existing algorithms with wavefront information provided by the level set method.

Recalling (2.4), if the phase function S takes the form $S(t, \mathbf{x}) = \tau(\mathbf{x}) - t$, substituting (2.2) into (2.1) results in the Helmholtz equation and associated frequency domain equation for the phase, $|\nabla \tau|^2 = \frac{1}{c^2(\mathbf{x})}$, and amplitude:

$$2\nabla \tau \cdot \nabla A_0 + (\nabla^2 \tau) A_0 = 0. \quad (2.14)$$

Parameterizing in terms of arclength s , the ray trajectory $\mathbf{x}(s)$ is defined as $\frac{d\mathbf{x}}{ds} = c\nabla\tau$. Rewriting the transport equation in terms of s gives [16]

$$2\frac{dA_0}{ds} + \left[\frac{c}{\hat{f}} \frac{d}{ds} \left(\frac{\hat{f}}{c} \right) \right] A_0 = 0, \quad (2.15)$$

which has the solution

$$A_0(s) = A_0(0) \left| \frac{c(s)\hat{f}(0)}{c(0)\hat{f}(s)} \right|^{1/2}, \quad (2.16)$$

where s is the arclength parameter, and \hat{f} is the Jacobian determinant describing the spreading of a "ray tube" in terms of the ray arclength, s . This Jacobian is given as $\left| \frac{\partial \mathbf{x}}{\partial (s, \gamma, \phi_1)} \right|$ with γ and ϕ_1 as the initial declination and azimuthal angles of the ray, respectively [16]. Typically the declination angle at the source is denoted θ , but γ is used here to avoid confusion with the independent variable θ used in the level set method. Converting to cylindrical coordinates and assuming azimuthal symmetry gives

$$\hat{f} = r \sqrt{\left(\frac{\partial z}{\partial \gamma} \right)^2 + \left(\frac{\partial r}{\partial \gamma} \right)^2}.$$

The key step in computing the amplitude using this approach is to compute the value of the Jacobian. Section 3 proposes a method for approximating (2.16) by using the solution provided by the level set method to compute the Jacobian \hat{f} .

3 Implementation

3.1 Solving the level set equations for underwater acoustics

The implementation discussed in this work is for computing the phase function in two-dimensional propagation. Eq. (2.10) is solved in Cartesian coordinates with a uniform line source, parallel to the y -axis as in Fig. 3, with z representing the water depth. Thus, the wave equation is reduced by symmetry to two dimensions given by (x, z) , where $z=0$ at the surface, and increases with increasing depth. If azimuthal symmetry is present in the domain and sound speed profile, a range-depth solution can be obtained by restricting to the right half of the x - z plane. Take the source to be located at $(0, z_s)$, then the level set functions can be initialized by setting

$$\phi_1(0, x, z, \theta) = x, \quad (3.1a)$$

$$\phi_2(0, x, z, \theta) = z - z_s. \quad (3.1b)$$

Solving the level set equations equates to solving a first order transport equation with variable coefficients in the reduced phase space, (x, z, θ) :

$$f_t + c(x, z) \cos(\theta) f_x + c(x, z) \sin(\theta) f_z + (c_x \sin(\theta) - c_z \cos(\theta)) f_\theta = 0. \quad (3.2)$$

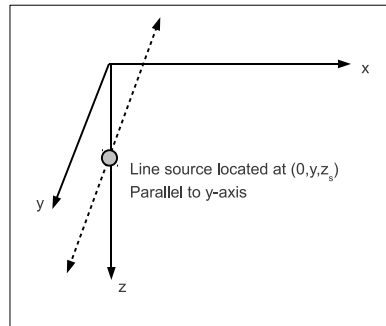


Figure 3: Sample problem geometry: a uniform line source parallel to the y -axis.

Eq. (3.2) is a Hamilton-Jacobi equation which can be solved using upwind finite differences as described in [20]. The complications arise from the boundary conditions. In this work, two types of boundary conditions have been applied: pure reflection and absorbing. The absorbing condition is handled naturally; the wavefront simply flows out of the domain. However, recall that the level set equations are solved in the full domain and for all $-\pi \leq \theta < \pi$, hence an inflow condition must be imposed at the boundary. One way to do this is to modify the differencing at inflow to use only data within the truncated domain. Alternately one could impose a zero flow Neumann condition.

The domain truncation at inflow will distort the solution near these boundaries, and the effect will worsen over time. In this level set method, only the intersection of zero level sets, representing the wavefront, is of interest. Since the wavefront propagates away from the source, the distortion at inflow is sufficiently removed from the zero level set. That is, perturbations to the level set function far from the wavefront do not affect the zero level set. It is important to keep in mind though that for very long time integration or for very sparse grids, the level set functions may need to be re-initialized periodically to prevent distortion of data close to the wavefront. For a discussion of reinitialization, see [1].

The reflection boundary condition poses a slight complication. To impose a reflection boundary condition at, say, the surface $\{z=0\}$, set [9]

$$\phi_1(t, x, 0, \theta_{refl}) = \phi_1(t, x, 0, \theta_{inc}), \quad (3.3a)$$

$$\phi_2(t, x, 0, \theta_{refl}) = \phi_2(t, x, 0, \theta_{inc}), \quad (3.3b)$$

$$\theta_{refl} = -\theta_{inc} \quad (3.3c)$$

in accordance with Snell's Law. Here, θ_{inc} and θ_{refl} are, respectively, the angles incident upon and reflected from the surface. For a general boundary, the condition would be

$$\theta_{refl} = 2\theta_B - \theta_{inc} - \pi, \quad (3.4)$$

where θ_B is the angle of the outward normal to the reflecting surface. This construction, under the velocity field given by (2.11) results in a sharp cusp at the boundary that grows

like $2c_0t$ in the case of a constant sound speed $c(x,z) = c_0$, at vertical incidence. This can be seen by recognizing that under a constant wave speed, (2.10) has the solutions

$$\begin{aligned}\phi_1(t,x,z,\theta) &= x - c_0t\cos\theta, \\ \phi_2(t,x,z,\theta) &= z - z_s - c_0t\sin\theta.\end{aligned}$$

Of course, vertical incidence is a worst-case scenario; at less severe angles, the vertical component of the velocity field, $c_0\sin\theta$, is reduced in magnitude. However, the singularity will worsen in severity for higher sound speeds and for longer periods of time integration. Such features may produce spurious oscillations when standard finite differencing methods are used. To mitigate this issue, a Weighted Essentially Non-Oscillatory (WENO) [21] interpolation based method is employed to obtain the spatial derivatives, and this is coupled with Total Variation Diminishing Runge-Kutta (TVDRK) [22] time integration. The first order TVDRK is equivalent to Forward Euler. These are Runge-Kutta methods designed to ensure that oscillations in the numerical approximation diminish over time. It is also necessary to be careful about interpolating in θ near the boundary for this reason. For this purpose, coefficients for WENO interpolation at an arbitrary point were derived and are presented in the Appendix.

WENO methods are high order methods; while higher order methods generally involve more computational work per grid point, there is a trade-off in that high order solvers require fewer grid points to meet a given error tolerance. To compute the time derivatives, first, second, and third order TVDRK methods are used. The WENO solvers that have been implemented for this work have orders $\nu=1,3$, or 5. The subsequent examples were produced using a combination of fifth order WENO and third order TVDRK. WENO methods are discussed further in the Appendix; for further details on TVDRK methods, the reader should refer to [22]. It is worth noting that Cheng proposes a semi-Lagrangian approach to propagating the level sets in phase space in [23]. In the present work, better performance was observed from the higher order WENO methods when the source was located close to a reflecting boundary.

The other matter with respect to boundary handling is the fact that the boundary location might not be in the (Cartesian) grid. One could use a non-uniform grid, but this affects the accuracy of the underlying WENO method. Instead, experimentation has shown that approximating the location of the boundary by the nearest grid points yields convergence. Two examples for which the boundary does not conform to the grid are presented in Section 4.

3.2 Solving the transport equation for the amplitude

In the level set method presented in this work for 2D propagation in the x - z plane, two level set functions $\phi_1(t,x,z,\theta)$ and $\phi_2(t,x,z,\theta)$ are defined in the reduced phase space $\subset \mathbb{R}^2 \times [-\pi,\pi]$, where θ gives the propagation direction of the wavefront (normal to the wavefront). Solving the level set equations for ϕ_1 and ϕ_2 , the wavefront can be extracted

as the intersection of the zero level sets of ϕ_1 and ϕ_2 . The objective is to use this information along with the initial condition in (2.15) to compute the solution given by (2.16). It is assumed at this point that no reflections occur; that is reserved for future extension.

3.2.1 Approach

Let $W(t) = \{\mathbf{x} | \phi_1(t, \mathbf{x}, \mathbf{k}) = \phi_2(t, \mathbf{x}, \mathbf{k}) = 0\}$ be the wavefront extracted from the level set method at time t . The goal is to compute the spreading loss at a given point $\mathbf{x}(t) \in W(t)$, where \mathbf{x} is specified in a Cartesian coordinate system, $\mathbf{x}(t) = (x(t), y(t), z(t))^T$. To solve the amplitude problem, the 3D scenario is considered with azimuthal symmetry and spherical spreading. Cylindrical spreading can also be treated (line source) with appropriate modification to the Jacobian. Suppose the loss is known along the wavefront at the previous time step, $W(t - \Delta t)$, and identify $\mathbf{x}(t - \Delta t)$ with \mathbf{x}_0 . Then in light of the above, it can be written that [13]

$$A(\mathbf{x}(t)) = A(\mathbf{x}_0) \frac{c(\mathbf{x}(t))}{c(\mathbf{x}_0)} \sqrt{\left| \frac{J(0)}{J(\Delta t)} \right|}. \quad (3.5)$$

In this notation, t is the ray parameter, and $\mathbf{x}(t)$ is the ray trajectory, that is, the point on the wavefront at the current time t evolved according to the ray direction from the point $\mathbf{x}(t - \Delta t) = \mathbf{x}_0$. The Jacobian in this formulation is given based on a time parameterization. It is convenient to use time as a parameter here since the level sets formulation is in the time domain. Since the initial condition is at time $t - \Delta t$, the Jacobian is evaluated for one time step. By definition, $J(0) = 1$. If $c(\mathbf{x}(t))$ is constant, then the rays are simply radial lines directed away from the source.

If the sound speed varies slowly with respect to the time evolution of the wavefront, the sound speed can be approximated as locally constant. Assume, without loss of generality, that the acoustic source is located at the origin. Let \mathbf{x} be a point on the wavefront at which the loss is to be computed, at some time $t = n\Delta t$, with $n > 1$ a positive integer. A ray can be traced back one time step using an ODE integrator (this is essentially a semi-Lagrangian scheme) to find the point on the wavefront, along that ray, at the previous time corresponding to \mathbf{x} , call this point \mathbf{x}_0 . Now let $\mathbf{y} = \mathbf{x} - \mathbf{x}_0$, and let $\bar{c} = c(\mathbf{x}_0)$ be the wave speed at the location \mathbf{x}_0 , which is assumed to be locally constant. Then this ray has the exact form

$$\mathbf{y}(t) = \mathbf{y}_0 + \bar{c}t \frac{\mathbf{y}_0}{|\mathbf{y}_0|} \quad (3.6)$$

and the Jacobian matrix is

$$\mathbf{I} + t \frac{\bar{c}}{|\mathbf{y}_0|} \left(\mathbf{I} - \frac{\mathbf{y}_0 \mathbf{y}_0^T}{|\mathbf{y}_0|^2} \right). \quad (3.7)$$

It is assumed here that $\mathbf{y}_0 \neq 0$ is an arbitrary point along the ray from the origin to \mathbf{y} . The Jacobian determinant J of the transformation from \mathbf{y}_0 at time $t=0$ to $\mathbf{y}(t)$ is given as

$$J(t) = \left(1 + t \frac{\bar{c}}{|\mathbf{y}_0|} \right)^2. \quad (3.8)$$

Expression (3.8) describes spherical spreading of rays in a medium with constant wave speed, and its value depends only on the distance of the starting location from the origin (source), and the distance traveled by a particle along the ray. It is independent of the actual location in space of the starting point (except that it cannot be evaluated directly for a ray starting at the origin).

To translate back to \mathbf{x} coordinates, take $\mathbf{y}_0 = \epsilon \frac{\mathbf{y}}{|\mathbf{y}|}$ where $\epsilon > 0$ is small. Then \mathbf{y}_0 maps to a starting point $\mathbf{x}_0 + \epsilon \frac{\mathbf{x} - \mathbf{x}_0}{|\mathbf{x} - \mathbf{x}_0|}$. Evaluate (3.8) at $t^* = \Delta t - \frac{\epsilon}{\bar{c}}$ so that the evaluation point maps to the desired location \mathbf{x} , and let $\epsilon \rightarrow 0$, yielding

$$\begin{aligned}
 J(\Delta t) &= \lim_{\epsilon \rightarrow 0} \left(1 + \left(\Delta t - \frac{\epsilon}{\bar{c}} \right) \frac{\bar{c}}{\left| \mathbf{x}_0 + \epsilon \frac{\mathbf{x} - \mathbf{x}_0}{|\mathbf{x} - \mathbf{x}_0|} \right|} \right)^2 \\
 &= \left(1 + \frac{\Delta t \bar{c}}{|\mathbf{x}_0|} \right)^2.
 \end{aligned}
 \tag{3.9}$$

Substituting the above into (3.5) yields

$$A(\mathbf{x}(t)) = A(\mathbf{x}_0) \frac{|\mathbf{x}_0|}{|\mathbf{x}_0| + \bar{c}\Delta t}.
 \tag{3.10}$$

Since it was assumed that $c(\mathbf{x})$ is constant along the ray from \mathbf{x}_0 to \mathbf{x} , the term from (3.5) involving the sound speed cancels.

Eq. (3.9) is only valid locally, so consider N rays corresponding to wavefront locations at time t given by $\{\mathbf{x}^i\}_{i=1}^N$. These locations correspond to N locations on the wavefront at time $t - \Delta t$, given by $\{\mathbf{x}_0^i\}_{i=1}^N$. Let c_i denote the constant sound speed value for ray i . To compute the spherical spreading, express $\mathbf{x}_0^i = r_0^i (\cos \gamma^i \cos \phi^i, \cos \gamma^i \sin \phi^i, \sin \gamma^i)$, with $r_0^i = |\mathbf{x}_0^i - \mathbf{x}_s|$ where \mathbf{x}_s is the source location. Then the spreading loss at the point $\mathbf{x}^i(t)$ along the wavefront is approximately

$$A(\mathbf{x}^i(t)) = A(\mathbf{x}_0^i) \frac{r_0^i}{r_0^i + c_i \Delta t}, \quad i = 1, \dots, N.
 \tag{3.11}$$

The value of $A(\mathbf{x}_0^i)$ can be estimated by interpolating the known values along the wavefront. For instance, if the wavefront is in the form of a circle in the x - z plane, it can be expressed as

$$A(x, y) = A((x - x_s) \cos(\theta), (z - z_s) \sin(\theta)),
 \tag{3.12}$$

where (x_s, y_s) is the source location, then interpolated in θ to obtain $A(\mathbf{x}_0^i) = A(\theta_0^i)$.

In the case of cylindrical spreading (line source), the Jacobian $J_{\text{cyl}}(\Delta t)$ is similarly given by

$$J_{\text{cyl}}(\Delta t) = 1 + \frac{\bar{c}\Delta t}{|\mathbf{x}_0|}.
 \tag{3.13}$$

The corresponding expression for the amplitude is

$$A(\mathbf{x}^i(t)) = A(\mathbf{x}_0^i) \sqrt{\frac{r_0^i}{r_0^i + c_i \Delta t}}. \quad (3.14)$$

3.2.2 Initialization

The preceding derivation assumes that the function $A(\mathbf{x})$ is known on $W(t - \Delta t)$. That information can be used to step forward in time to evolve the amplitude along with the level sets, or as post-processing. At $t = 0$, the initial condition to the wave equation is taken as a point source located in space at $\mathbf{x}_s = (x_s, y_s, z_s)$, or in the 2D formulation in the x - z plane, the source is located at $\mathbf{x}_s = (x_s, z_s)$. The source is associated with some initial, known, source level, A_{source} . The Jacobian is not defined at the source, so another technique must be used. To initialize the procedure, proceed as in [16]. The exact solution for the pressure field due to a point source in an unbounded, homogeneous medium with sound speed c_0 is proportional to

$$p(\mathbf{x}(t)) = -S_\omega \frac{e^{i\omega t}}{4\pi c_0 t}. \quad (3.15)$$

The value S_ω represents a known source strength, in terms of the surface displacement of a small, spherical source, and is proportional to A_{source} . Given the general form of the pressure,

$$p(\mathbf{x}) = A(\mathbf{x}) e^{i\omega\tau(\mathbf{x})}, \quad (3.16)$$

it can be deduced that

$$A(\mathbf{x}(\Delta t)) = -S_\omega \frac{1}{4\pi c_0 \Delta t}. \quad (3.17)$$

3.2.3 Algorithm

An outline of the algorithm for computing the amplitude using the ray-based procedure for 2D propagation in the x - z plane is given below. Suppose there is a known set of points $\{\mathbf{x}_0^i\}_{i=0}^N$ along a wavefront at a time t_0 , the values of $A(\mathbf{x}_0^i(t_0))$ for $i = 1, \dots, N$, and a set of points along the evolved wavefront, $\{\mathbf{x}_1^i\}_{i=0}^M$ at time $t_1 = t_0 + \Delta t$, the following steps are used to compute $A(\mathbf{x}_1^i(t_1))$, $i = 1, \dots, M$. Let $\mathbf{x}_1^i = (x_1^i(t), z_1^i(t))$. Then,

1. Solve the backward ray equations in the time domain:

$$\begin{aligned} \dot{x}(t) &= c(\mathbf{x}(t)) \cos\theta(t), \\ \dot{z}(t) &= c(\mathbf{x}(t)) \sin\theta(t), \\ \dot{\theta}(t) &= \frac{\partial c}{\partial x} \sin\theta(t) - \frac{\partial c}{\partial z} \cos\theta(t), \end{aligned}$$

subject to $x^i(t_1) = x_1^i$ and $z^i(t_1) = z_1^i$. Also assume $\theta^i(t_1)$ for $i = 1, \dots, M$ is available from the level set data. This solve can be implemented using a simple Euler method backward in time as

$$\begin{aligned}x^i(t_0) &= x_1^i - c(\mathbf{x}_1^i) \Delta t \cos \theta^i(t_1), \\z^i(t_0) &= z_1^i - c(\mathbf{x}_1^i) \Delta t \sin \theta^i(t_1), \\\theta^i(t_0) &= \theta^i(t_1) - \Delta t V_\theta,\end{aligned}$$

where

$$V_\theta = \left. \frac{\partial c}{\partial x} \right|_{\mathbf{x}_1^i} \sin \theta^i(t_1) - \left. \frac{\partial c}{\partial z} \right|_{\mathbf{x}_1^i} \cos \theta^i(t_1).$$

Note that the sound speed is assumed to be smooth so that these derivatives exist. A higher order method could be applied, but in the general case may require a nonlinear solve depending on the form of c . A first order method is used here due to its simplicity and the fact that the wavefront locations are only available to first order.

2. Compute the range from the acoustic source to $\mathbf{x}^i(t_0)$ for $i = 1, \dots, N$:

$$r_0^i = \sqrt{(x^i(t_0) - x_s)^2 + (z^i(t_0) - z_s)^2},$$

where the source is located at (x_s, z_s) .

3. If $t_1 = \Delta t$ (first step only), compute the arclength

$$s^i = \int_{t_0}^{t_1} c(\mathbf{x}^i(t)) dt$$

for each ray, $\mathbf{x}^i(t)$.

4. Consider the amplitude along the wavefront at t_0 to be a function of the phase space variable θ , $A = A(\theta(t))$ and interpolate to find $A(\theta^i(t_0))$ for each i . This breaks down when the wavefront bounces or runs outside of the domain. Addressing that case is set aside for future work.

5. If $t_1 > \Delta t$, set

$$A(\mathbf{x}_1^i) = A(\mathbf{x}_0^i) \frac{r_0^i}{r_0^i + \Delta t c(\mathbf{x}_0^i)}.$$

Otherwise, set

$$A(\mathbf{x}_1^i) = A_{\text{source}} \frac{1}{s^i}.$$

6. Step forward in time and repeat.

3.2.4 Remark

The proposed approach to computing the amplitude has very nice stability properties. Assuming that a linear (or other well-behaved) interpolation scheme is applied to the amplitudes at time $t - \Delta t$, the result $A(\mathbf{x}(t)) \leq A(\mathbf{x}(t - \Delta t))$ holds for any Δt . This is a standard result for semi-Lagrangian type methods. However if Δt is allowed to be too large, the accuracy will suffer from the constant wave speed approximation. This result

will not apply when A blows up due to a caustic; handling of caustics is a challenge left to future work, possibly by adapting the approaches of [24] or [25]. Both of these works use a Gaussian beam model to propagate the spreading loss; the GRAB (Gaussian Ray Bundles) [25] approach applies an empirically derived threshold to prevent blow-up at caustics. Since the proposed method is based on the Lagrangian form, these approaches could be applied directly as an enhancement. Caustics do not represent a numerical instability, but a consequence of the high frequency limit in the geometric optics approximation. By construction, this method will not lead to infinite amplitudes, but special treatment will be necessary to produce accurate approximations in the vicinity of and beyond caustics.

4 Results

In this section, some computational results are presented to show convergence of the wavefronts computed using the level set method, and compare the solutions to those of the full wave equation.

4.1 Comparison to exact solutions

The examples in this section are test cases for which analytical solutions are available to study convergence. Results for two sound speed profiles are presented in the absence of reflections from surface or bottom. The results are based on implementation of a fifth order WENO scheme coupled with third order TVD Runge-Kutta time integration on an $N \times N \times N$ grid. Comparison is made with the exact solutions after 0.1 seconds and errors are reported in the max norm, evaluated in a fixed neighborhood of the wavefront (and for the linear profile example, away from vertical angles where the exact solution is poorly behaved). The theoretical convergence rate is not observed immediately, but even for comparatively sparse grids, observed convergence is faster than first order.

4.1.1 Isovelocity profile

This example uses $c = 1.0$ km/s, independent of location in space, and a point source at $z = z_s = 0.5$ km with $x \in [-1, 1]$ and $z \in [0, 1]$. In this case the characteristics are straight lines so $\theta(t) = \theta_0$ and the solutions to the level set equations are given as $\phi_1(t, x, z, \theta) = x - t \cos(\theta)$, and $\phi_2(t, x, z, \theta) = z - z_s - t \sin(\theta)$. The results, evaluated at $t = 0.1$ s and without reflection, are presented in Table 1.

Initially, the solution appears to be converging like $\frac{1}{N^2}$. The expected fifth order convergence is observed at $N = 160$, then the error decreases even more rapidly as N is increased to 320.

Table 1: Accuracy analysis 1: $c = \text{constant}$.

N	Error (max norm)	Effective Order
20	3.306945E-03	–
40	8.509789E-04	1.96
80	1.164058E-04	2.87
160	2.695106E-06	5.43
320	2.312644E-09	10.19

4.1.2 Linear profile

An exact solution to the level set equations is available for the case of a profile linear in depth: $c(z) = \alpha z + \beta$, where α and β are constants. For this example, $\alpha = 0.5$ and $\beta = 1.0$ are chosen, where units are again in km/s. The initial condition is a point source at $z = z_s = 0.5$ km with $x \in [-1, 1]$ and $z \in [0, 1]$. The exact solution for this case is given (away from $\theta = \frac{\pi}{2}$) by

$$\phi_1(t, x, z, \theta) = x + \hat{\gamma} \left(z + \frac{\beta}{\alpha} \right) \frac{1 - e^{2\alpha t}}{1 + \hat{\gamma}^2 e^{2\alpha t}}, \quad (4.1)$$

$$\phi_2(t, x, z, \theta) = \left(z + \frac{\beta}{\alpha} \right) \frac{(1 + \hat{\gamma}^2) e^{\alpha t}}{1 + \hat{\gamma}^2 e^{2\alpha t}} - \frac{\beta}{\alpha} - z_s, \quad (4.2)$$

where

$$\hat{\gamma} = \tan \left(\frac{\theta}{2} + \frac{\pi}{4} \right). \quad (4.3)$$

The results of this investigation are presented in Table 2.

Table 2: Accuracy analysis 2: $c(z)$ linear.

N	Error (max norm)	Effective Order
20	5.253662E-03	–
40	3.423236E-03	0.62
80	4.712438E-04	2.86
160	1.382231E-05	5.09
320	5.375073E-08	8.01

The observed convergence rate is somewhat slower in this case than for the isovelocity profile, but still fifth order convergence is observed at $N = 160$ and rapidly begins to approach the true solution for larger N . The slower convergence in this case is likely due to the fact that the isovelocity problem is actually a two-dimensional problem in the phase space, since the direction of travel, θ , is constant and hence the θ component of the velocity field is zero. When a variable sound speed is introduced, the problem is fully three-dimensional.

4.2 Examples involving reflection

This section presents computational results for profiles with reflecting boundaries. The examples with grid-conforming boundaries were computed using a $50 \times 50 \times 50$ grid. The examples with sloping boundaries use an $80 \times 80 \times 80$ grid. The format for presenting the results in Figures 4 to 6 is time snapshots of the wavefront superimposed on contours from a full wave equation result for the same profile and ocean geometry. Including the amplitude contours from a finite frequency full wave solver serves as a check on the accuracy of the solutions. The profiles used were selected for theoretical illustration and are not realistic ocean profiles.

4.2.1 Linear in depth and range profile with flat, reflecting bottom

Fig. 4 applies a profile linear in both x and z : $c(x,z) = 0.5x + 0.5z + c_0$ to the same scenario. This example serves to illustrate that sound speed range dependence is a natural feature of this algorithm. The full wave equation solver is a finite frequency solution so it does not produce wavefronts exactly, but the wavefront is located where the contours appear to be converging together, corresponding to a rapid change in amplitude. The thick, black line representing the wavefront computed at each specified time step is seen to lie right on the leading edge of the converging contours, as expected, even after multiple reflections.

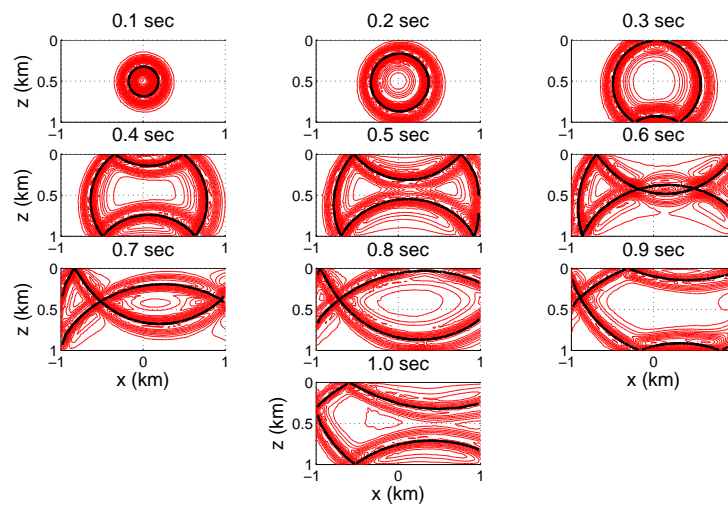


Figure 4: Time snapshots of wavefronts (thick, black curve) computed using level sets, superimposed on full field amplitude contours: $c(x,z) = 0.5x + 0.5z + c_0$ km/s.

4.2.2 Isovelocity profile with sloping bottom

The next two examples are included to illustrate the handling of a bottom geometry that is dependent on the x variable. The simplest such type of domain incorporates a slop-

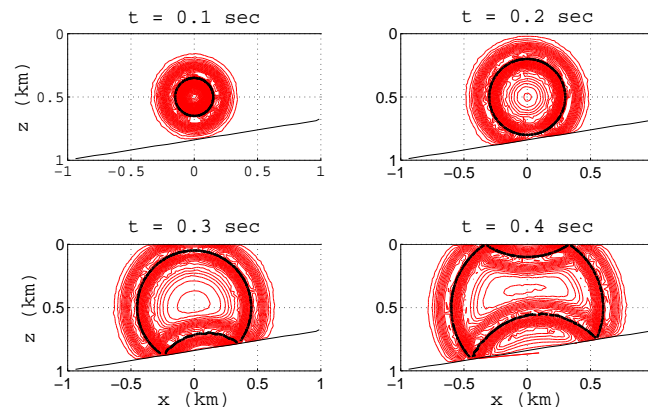


Figure 5: Time snapshots of wavefronts (thick, black curve) computed using level sets, superimposed on full field amplitude contours: 9° upslope.

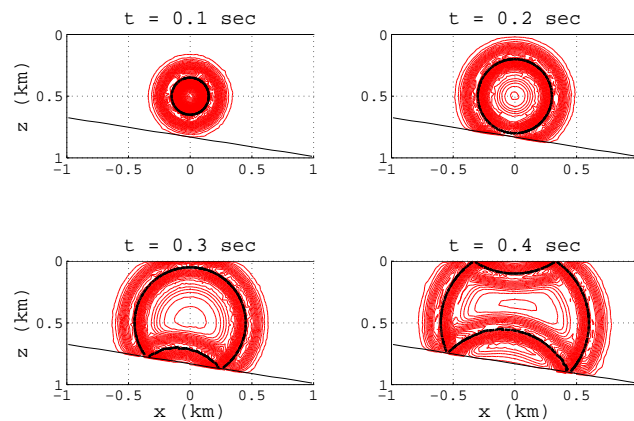


Figure 6: Time snapshots of wavefronts (thick, black curve) computed using level sets, superimposed on full field amplitude contours: 9° downslope.

ing bottom. Fig. 5 shows the results with an upslope of 9° from horizontal, while Fig. 6 was produced with a downslope of 9° from horizontal. The computational challenge presented by this case is the representation of a boundary that does not conform to the Cartesian grid employed to extract the desired convergence rate from the WENO method which is heavily dependent on uniform grid spacing, or equivalently, a smooth mapping to a uniform grid. Through experimentation, it was discovered that greater stability was achieved by implementing the boundary condition at the nearest grid point to the physical boundary location, rather than modifying the grid to include the boundary. Although this results in some irregularity in the extracted wavefronts post-reflection, the figures indicate a very nice match with the apparent true wavefront location. The boundary effects have been shown to be reduced as the grid is resolved. Both examples use the sound speed $c = 1.5$ km/s, a reasonable value for a shallow water ocean environment [26].

4.3 Example with variable sound speed profile

4.3.1 Propagation in a channel

In this example, a profile that simulates a waveguide presents an interesting comparison between the ray trace and wavefront models. The model is an acoustic analog of the quantum harmonic oscillator, discussed in more detail by Foreman [27]. This profile yields a normal mode solution that is tractable at low frequencies, but the behavior becomes more complicated in the high frequency limit. A source is placed at $z_s = 0.5$ km in a field with

$$c(z) = \frac{c_0}{\sqrt{1 - \left(1 - \frac{z}{z_s}\right)^2}},$$

and a sound speed of $c_0 = 1.5$ km/s (Fig. 7) at the source depth. This scenario represents a waveguide, symmetric about the sound channel axis at $z = z_s$, as $c(z)$ approaches infinity at the channel boundaries $z = 0$ km and $z = 1$ km. The rays are oscillating functions about the sound channel axis. In the wavefront model, this corresponds to a periodically self-crossing wavefront. Fig. 8 shows snapshots of the wavefront computed using the level set technique with wavefronts extracted from a ray trace superimposed for validation. The match is very good away from the source. The errors are greater closer to the source, but this can be resolved by using a finer grid in the level set implementation.

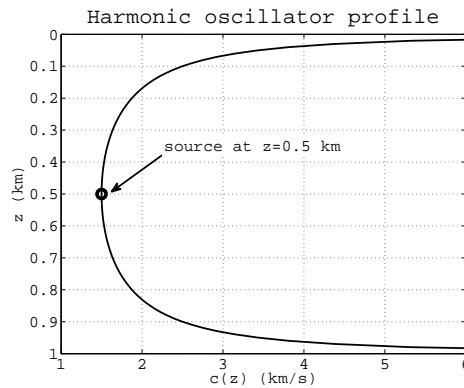


Figure 7: Sound speed as a function of depth for harmonic oscillator profile.

4.4 Examples with scattering

4.4.1 Scattering off bottom features

The following examples explore range dependence a little further by introducing rectangular (grid-conforming) features in the domain. In order to avoid overcomplicating the scenarios, the sound speed profile was held constant at $c = 1.5$ km/s. In Fig. 9, a rectangular scatterer is placed on the "ocean" bottom. As would be expected from a pure geo-

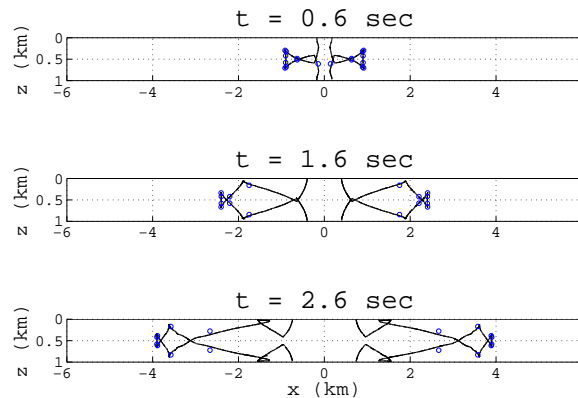


Figure 8: A subset of the time snapshots of wavefronts computed using level sets: $c(z) = c_0 / (\sqrt{1 - (1 - z/z_s)^2})$, with wavefronts extracted from an analogous ray trace appearing as circles superimposed on the level sets wavefronts.

metric optics approximation, the diffraction at the corner is not represented by the level set method. Away from the corner, the results agree nicely with the full wave equation model, however a spurious zero level set appears in the phase space when the wavefront reflects off of the object. This can be understood more easily by considering a plane wave source. Recall that the wavefront is represented in the model as the intersection of zero level sets of two functions. Thus the function is positive on one side of the front, say the leading part and negative on the other (lagging). When part of the wavefront reflects off the object, the positive values reflect back in the opposite direction in the phase space, but the part that does not encounter the object retains the same sign in that direction, creating a discontinuity. Because there is a change of sign over this discontinuity, a zero level set exists as an artifact. One could apply edge detection to remove this artifact, but that is not terribly reliable as an approach because it is difficult to distinguish numerically between a discontinuity and a steep gradient in a smooth function. Instead, since this is a non-physical effect, a proper computation of the amplitude, when incorporated, should assign negligible weight to those locations along the computed wavefront.

4.4.2 Scattering from an obstacle

This final example, in Fig. 10, is included to demonstrate a potentially useful application for an acoustic level set method. The rectangular geometry is kept for the sake of conforming to the grid, but this time the scatterer is an object in a domain with absorbing boundaries, which could represent an object in the deep ocean. The point source is located at $z_s = 0.5$ km and the sound speed is again $c = 1.5$ km/s. This example also suffers from the same effects as the above examples (i.e., the spurious zero level sets upon reflection). However this example really demonstrates how this method changes the point of view for a scattering problem from the ray-based situation to having the ability to fully

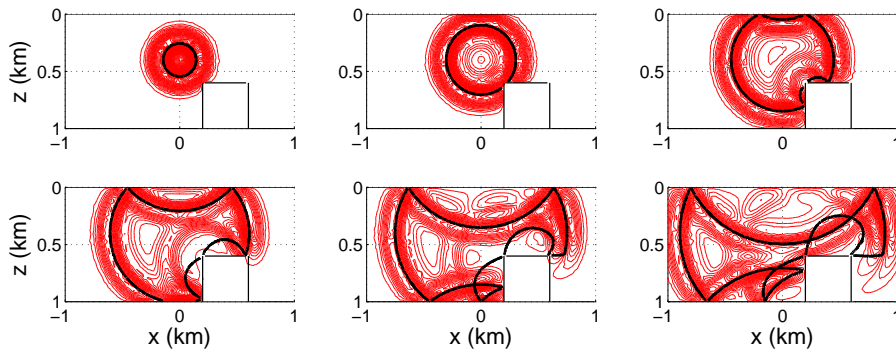


Figure 9: Time snapshots of wavefronts (thick, black curve) computed using level sets in the presence of a rectangular bottom scatterer.

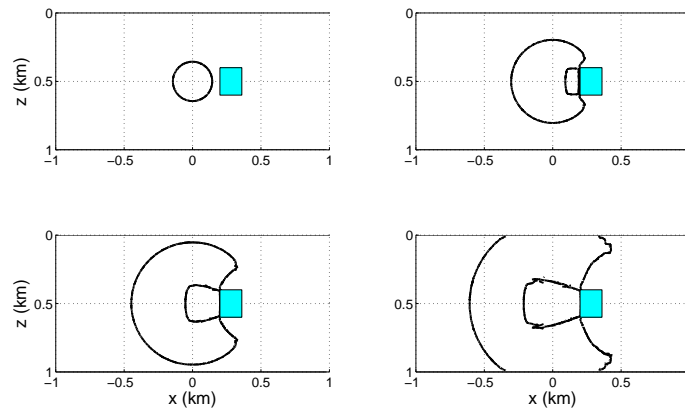


Figure 10: Time snapshots of wavefronts computed using level sets in the presence of a scattering obstacle in the domain.

capture shape information from acoustic reflection off an object. A ray-based model involves the specification of locations on the object, dependent upon its orientation if it's not spherically symmetric, to which to trace eigenrays in order to simulate a response. Using a wavefront model, one can fully utilize the object's shape information and avoid having to compute eigenrays.

4.5 Validation of the spreading loss

In this subsection, some computational results are presented to show convergence of the wavefronts computed using the level set method, and compare the solutions to those of the full wave equation. A few test cases have been prepared to validate that the proposed algorithm for computing the spreading loss from the wavefronts resulting from the level set method procedure produces an acceptable result. A comparison with the theoretical spreading loss in an isovelocity environment (Fig. 11) with $c = 1.5$ km/s shows excellent

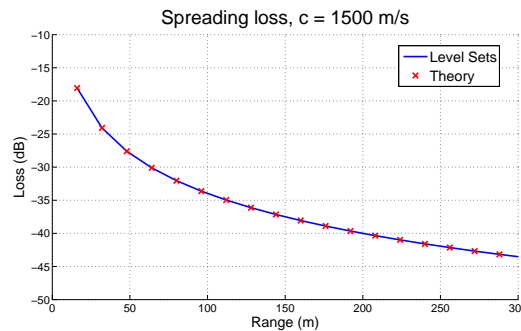


Figure 11: Level set method wavefront amplitude as a function of range compared to theoretical result.

agreement from the method outlined in Section 3.2. The agreement is expected in this case since the constant sound speed assumption holds everywhere.

Further comparisons were also performed using the amplitudes computed using the RAY [28] software package. In each case, a point source is located at $z_s = 0.5$ km with $z \in [0,1]$ km. Under the assumptions of no surface or bottom bounces (deep water only) and short time propagation (so no crossing rays), wavefront data were extracted and accumulated over time and the amplitudes interpolated to produce Figs. 12, 14, and 16. Accompanying these figures, Figs. 13, 15, and 17 show good agreement in direct comparisons of the fields computed along a horizontal slice at the source depth. Figs. 12 and 13 were generated with an isovelocity environment ($c = 1.5$ km/s). Figs. 14 and 15 result from a linear (in z) sound velocity given by $c(z) = 0.5z + c_0$, with $c_0 = 1.5$ km/s. Figs. 16 and 17 display results using the sound velocity profile

$$c(z) = \frac{c_0}{\sqrt{1 + 2.4z/c_0}},$$

with $c_0 = 1.55$ km/s.

5 Conclusion

Level set methods provide an alternative framework for numerical solutions to the high frequency approximation to the wave equation. A fixed-grid point of view is advantageous for medium range (about 1 kilometer), high frequency modeling. In particular, it is very difficult to compute accurate eigenray solutions for active sonar in shallow water environments with range-dependent bathymetric features. Another situation where level set methods will hold an advantage is when multiple sound sources and receivers are present. To find the arrival times or amplitudes at a location using rays, one would have to trace two-way ray paths (eigenrays) between each possible source/receiver pair. With an Eulerian approach, the sources can be embedded into a single level set function and the wavefronts propagated together. Time arrivals are identified with the times of simultaneous zero crossings of the components of the level set function at the receiver location(s).

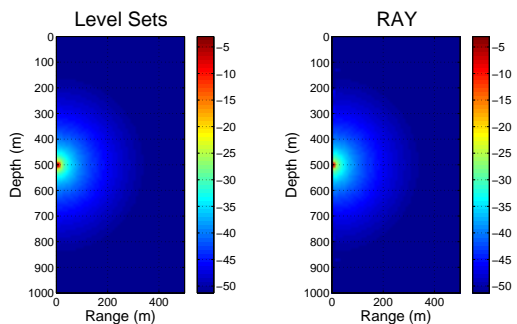


Figure 12: Spreading loss computed using Level Set Method (left) compared to extracted loss from RAY (right) for a constant sound speed.

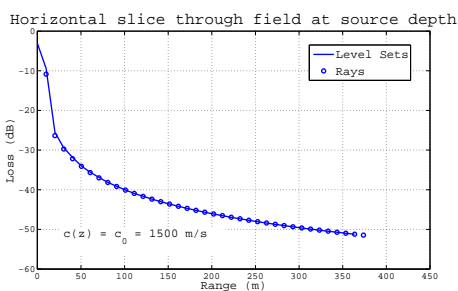


Figure 13: Spreading loss computed using Level Set Method (left) compared to extracted loss from RAY (right) for a constant sound speed.

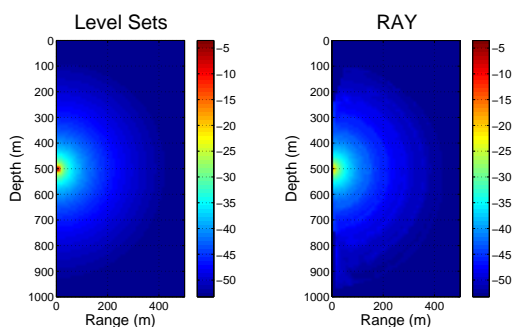


Figure 14: Spreading loss computed using Level Set Method (left) compared to extracted loss from RAY (right) for a sound speed function varying linearly in depth.

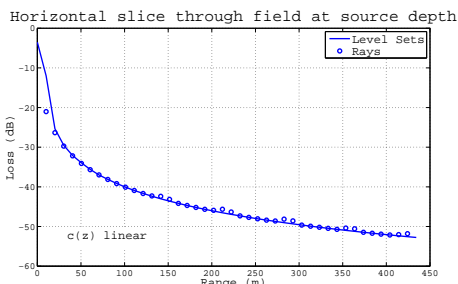


Figure 15: Spreading loss validation – horizontal slices through the fields shown in Fig. 14 at source depth.

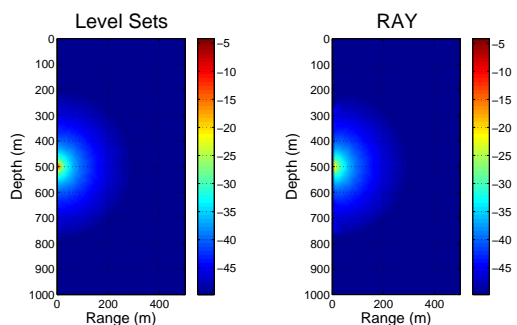


Figure 16: Spreading loss computed using Level Set Method (left) compared to extracted loss from RAY (right) for a sound speed function with square inverse varying linearly in depth (n^2 linear).

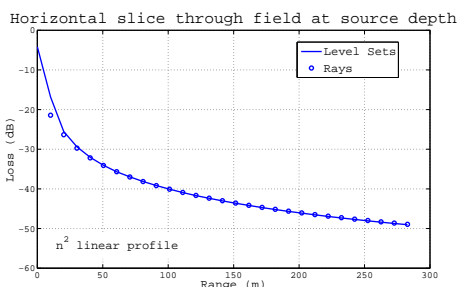


Figure 17: Spreading loss validation – horizontal slices through the fields shown in Fig. 16 at source depth.

This work has introduced a method that applies a level set formulation to the high frequency acoustics problem; the model was discussed in Section 2, its implementation described in Section 3, and some basic examples provided in Section 4 to validate the model and illustrate its capabilities. The effects of reflecting boundary conditions have been studied and appropriate methods employed to improve computational results in such domains. A limitation of the method was exposed wherein discontinuities in the level set function resulting from reflections off of an object in the domain leads to the detection of spurious zero level sets by the graphics processing routines. Reflections are an important consideration for shallow water acoustics, and a reasonable approximation at high frequencies where the amount of energy transmitted into the sea bottom is negligible. An efficient, ray-based approach to computing the spreading loss from the wavefront data has also been presented and validated in the absence of boundary reflections. There are several open issues left to future work. Certainly the computation of amplitude needs to be extended to handle reflections and also to incorporate scattering and attenuation losses to fully represent the pressure field. A fully three-dimensional propagation implementation would be useful and interesting. It would also be interesting to consider incorporating higher order effects (e.g., diffraction) into the model. Since the level set method and ray tracing are both based on the geometric optics approximation, the level set method also leads to unbounded amplitudes at caustics, so it would be worth investigating approaches to computing physically realistic amplitude values in such situations.

Acknowledgments

The author would like to thank Dr. Drumheller and Dr. Soukup of ONR for continued support of this program. This work is also a result of initial funding by the In-house Laboratory Independent Research (ILIR) program at Naval Undersea Warfare Center (NUWC), Newport, RI, and is partially funded by the Science, Mathematics, And Research for Transformation (SMART) program. I thank Dr. Jan Hesthaven of Brown University for his technical oversight and advice, Dr. Kevin Bongiovanni of Raytheon/BBN for suggesting this topic, and Dr. Andrew Fredricks also of NUWC for helpful guidance. Zhu Xueyu of Brown University contributed the Discontinuous Galerkin-Perfectly Matched Layers (DG-PML) full wave equation code to verify solutions. Ray trace results were obtained from the code RAY produced at Woods Hole Oceanographic Institute [28].

Appendix: Essentially Non-Oscillatory (ENO) and Weighted ENO (WENO) interpolation

In ENO interpolation, introduced by Harten et al. [29] and later refined by Shu and Osher [30,31], one seeks to choose an appropriate stencil on which to approximate a function, which may be only piecewise smooth, by Lagrange polynomials. The idea is to

isolate points of discontinuity, using a measure of the function's variation. That is, the stencil is adaptive, versus using a fixed stencil as in a standard interpolation routine. WENO interpolation, extends ENO by combining the results from all candidate stencils to achieve $\mathcal{O}(\Delta x^{2k-1})$ accuracy, where k is the accuracy order of the underlying ENO method. Only the one-dimensional problem is discussed here, but the extension to multiple dimensions for implementation of a level set method is straightforward. In particular, on the Cartesian grid, the same operations are performed in each dimension.

A.1 ENO finite difference reconstruction

As in Shu's comprehensive report [21], for polynomial reconstruction in one dimension, establish a uniform grid $\{x_{i-\frac{1}{2}}\}_{i=0}^N$, with $\Delta x = x_{\frac{1}{2}} - x_{-\frac{1}{2}}$. That the grid is uniform is critical for the finite difference formulation, but this requirement can be relaxed if a finite volume scheme is employed instead, or if a smooth transformation to a uniform grid is available. The present implementation is built on finite differences, so a uniform grid is assumed. Define the cells $I_i = [x_{i-\frac{1}{2}}, x_{i+\frac{1}{2}}]$ for $i=0, \dots, N-1$. Assume the values of the function $f(x)$ are available at the cell centers, $\{f(x_i) \equiv f_i\}_{i=0}^{N-1}$. The goal of ENO is to use these values to construct an approximation, $\hat{f}_{i+\frac{1}{2}}$, such that

$$\left. \frac{\partial f}{\partial x} \right|_{x_i} = \frac{\hat{f}_{i+\frac{1}{2}} - \hat{f}_{i-\frac{1}{2}}}{\Delta x} + \mathcal{O}(\Delta x^k). \quad (\text{A.1})$$

In the context of the simple conservation law $u_t + u_x = 0$, $\hat{f}_{i+\frac{1}{2}}$ can be viewed as a numerical flux function for $f(u) = u$.

For each cell I_i , define the k -point stencil $S_r(i)$:

$$S_r(i) = \{x_{i-r}, \dots, x_{i+s}\}, \quad (\text{A.2})$$

where $r+s+1 = k$. In ENO, one begins with a single cell stencil then adaptively adds points depending upon the value of some smoothness measure, e.g., the divided difference, so that r depends on the cell i . The function values f_i are viewed as the cell averages of some unknown function, $h(x)$:

$$f(x) = \frac{1}{\Delta x} \int_{x-\frac{\Delta x}{2}}^{x+\frac{\Delta x}{2}} h(\xi) d\xi. \quad (\text{A.3})$$

Take $H(x) = \int_{-\infty}^x h(\xi) d\xi$. Rather than directly approximating $f(x)$, the relationship of the implicitly defined function $h(x)$ to $f(x)$ is

$$f'(x) = \frac{1}{\Delta x} \left(h\left(x + \frac{\Delta x}{2}\right) - h\left(x - \frac{\Delta x}{2}\right) \right),$$

which allows one to define a flux function in terms of the reconstructed values of h at the cell edges, $\{h_{i+\frac{1}{2}}^-\}_{i=0}^{N-1}$ and $\{h_{i-\frac{1}{2}}^+\}_{i=0}^{N-1}$. The $-$ and $+$ superscripts indicate the limits from

the left and right, respectively. To find these approximations, seek a polynomial $p_i(x)$ defined on $S_r(i)$ such that p_i approximates h in the sense that

$$\frac{1}{\Delta x} \int_{x_{i-\frac{1}{2}}}^{x_{i+\frac{1}{2}}} p_i(\xi) d\xi = f_i. \tag{A.4}$$

To achieve an estimate satisfying (A.1), require that the polynomial p_i has degree at most $k-1$. Now define the primitive of p_i as $P_i(x) = \int_{-\infty}^x p_i(\xi) d\xi$. Then, $P_i(x)$ is related to f as

$$\frac{1}{\Delta x} \left(P_i(x_{i+\frac{1}{2}}) - P_i(x_{i-\frac{1}{2}}) \right) = f_i.$$

There is also the relationship

$$\begin{aligned} h_{i+\frac{1}{2}}^- &= p_i(x_{i+\frac{1}{2}}) = P_i'(x_{i+\frac{1}{2}}), \\ h_{i-\frac{1}{2}}^+ &= p_i(x_{i-\frac{1}{2}}) = P_i'(x_{i-\frac{1}{2}}). \end{aligned}$$

Take $P_i(x)$ to be the Lagrange polynomial interpolating the function $H(x)$ over the $k+1$ points $x_{i-r-1/2}, \dots, x_{i+s+1/2}$, so P_i satisfies

$$P_i(x) = \sum_{m=0}^k H(x_{i-r+m-1/2}) \ell_{i,r,m}^k(x).$$

The form of the Lagrange polynomial can be found in any basic numerical analysis text-book, and is represented here as

$$\ell_{i,r,m}^k(x) = \prod_{\substack{l=0 \\ l \neq m}}^k \frac{x - x_{i-r+l-1/2}}{x_{i-r+m-1/2} - x_{i-r+l-1/2}}.$$

To eliminate the dependence on the unknown function $H(x)$, write

$$\begin{aligned} P_i(x) - H(x_{i-r-1/2}) &= \sum_{m=0}^k (H(x_{i-r+m-1/2}) - H(x_{i-r-1/2})) \ell_{i,r,m}^k(x) \\ &= \sum_{m=1}^k \left(\sum_{j=0}^{m-1} f_{i-r+j} \Delta x \right) \ell_{i,r,m}^k(x), \end{aligned} \tag{A.5}$$

so that $P_i(x)$ is expressed in terms of the data, $\{f_j\}$. Upon differentiating (A.5), rearranging terms, and substituting $x = x_{i+1/2}$ and $x = x_{i-1/2}$, one can see that the reconstructed values on the stencil $S_r(i)$ have the form

$$h_{i+\frac{1}{2}}^- = \sum_{j=0}^{k-1} c_{rj} f_{i-r+j}, \quad h_{i-\frac{1}{2}}^+ = \sum_{j=0}^{k-1} \tilde{c}_{rj} f_{i-r+j}, \tag{A.6}$$

where the constants c_{rj} and \tilde{c}_{rj} are grid-dependent as derived from the derivatives of the Lagrange polynomials. Furthermore, given the definitions of $h_{i+\frac{1}{2}}^-$ and $h_{i+\frac{1}{2}}^+$ and the stencil $S_r(i)$, it is apparent that $\tilde{c}_{rj} = c_{r-1,j}$. The values of c_{rj} as presented in [21] are provided here for completeness in Table 3.

Table 3: Constants for reconstruction in (A.6), for $k=1,2,3$.

k	r	$j=0$	$j=1$	$j=2$
1	-1	1		
	0	1		
2	-1	$\frac{3}{2}$	$-\frac{1}{2}$	
	0	$\frac{1}{2}$	$\frac{1}{2}$	
	1	$-\frac{1}{2}$	$\frac{3}{2}$	
3	-1	$\frac{11}{6}$	$-\frac{7}{6}$	$\frac{1}{3}$
	0	$\frac{1}{3}$	$\frac{5}{6}$	$-\frac{1}{6}$
	1	$-\frac{1}{6}$	$\frac{5}{6}$	$\frac{1}{3}$
	2	$\frac{1}{3}$	$-\frac{7}{6}$	$\frac{11}{6}$

A.2 WENO finite difference reconstruction

WENO is an extension of ENO, based on the observation that ENO adaptively selects a single stencil for each cell and so effectively uses $2k-1$ cells to obtain order k accuracy. Instead, Liu, Osher, and Chan [32] proposed that all candidate stencils be combined into an order $2k-1$ accurate reconstruction. This is accomplished by defining weights on each stencil so that approximations on stencils where the function appears to be smooth are given a significant weight and those in stencils containing a discontinuity are given very small weight. Let $h_{i+1/2}^{(r)}$ represent the reconstruction on the r^{th} stencil $S_r(i) = \{x_{i-r}, \dots, x_{i-r+k-1}\}$, that is, using (A.6),

$$h_{i+1/2}^{(r)} = \sum_{j=0}^{k-1} c_{rj} f_{i-r+j}, \quad r=0, \dots, k-1. \tag{A.7}$$

Then there are weights ω_r satisfying $\omega_r \geq 0$ and $\sum_{r=0}^{k-1} \omega_r = 1$ such that

$$h_{i+1/2} = \sum_{r=0}^{k-1} \omega_r h_{i+1/2}^{(r)} = h(x_{i+1/2}) + \mathcal{O}(\Delta x^{2k-1}).$$

A Taylor expansion,

$$h_{i+1/2} = \sum_{r=0}^{k-1} d_r h_{i+1/2}^{(r)}, \quad h_{i-1/2} = \sum_{r=0}^{k-1} d_{k-1-r} h_{i-1/2}^{(r)} \tag{A.8}$$

Table 4: Constants d_r from (A.8), for $k=1,2,3$.

k	d_0	d_1	d_2
1	1	-	-
2	$\frac{2}{3}$	$\frac{1}{3}$	-
3	$\frac{3}{10}$	$\frac{3}{5}$	$\frac{1}{10}$

approximates $h(x_{i+1/2})$ and $h(x_{i-1/2})$ (by symmetry) with error $\mathcal{O}(\Delta x^{2k-1})$. The constants d_r are repeated from [21] in Table 4 for completeness.

When the stencil contains a discontinuity, it is desired that the stencil be assigned a weight $\omega_r \ll 1$, and in smooth regions $\omega_r \approx d_r$. The weights take the form

$$\omega_r = \frac{\alpha_r}{\sum_{s=0}^{k-1} \alpha_s} \quad (\text{A.9})$$

for $r=0, \dots, k-1$, where

$$\alpha_r = \frac{d_r}{(\epsilon + \beta_r)}, \quad \tilde{\alpha}_r = \frac{d_{k-1-r}}{(\epsilon + \beta_r)^2}. \quad (\text{A.10})$$

Here β_r is the smoothness factor, and ϵ is just a small constant to prevent division by zero. A choice for β_r is given in [33] that is based on the variation of the reconstruction polynomial $p_r(x)$ defined by stencil $S_r(i)$ in cell I_i :

$$\beta_r = \sum_{l=1}^{k-1} \int_{x_{i-1/2}}^{x_{i+1/2}} \Delta x^{2l-1} \left(\frac{\partial p_r(x)}{\partial x} \right)^2 dx. \quad (\text{A.11})$$

The expressions for computing β_r from the function values $\{f_i\}_{i=0}^{N-1}$ can be derived from the form of the reconstruction polynomial, or refer to [21]. The WENO procedure is summarized in Algorithm 1.

Algorithm 1 WENO Reconstruction of $h_{i-1/2}^+$, $h_{i+1/2}^-$

Require: $i \geq 0$, data $\{f_{i+r}\}_{r=-k}^k$, $\epsilon > 0$ $\{\epsilon = 10^{-6}$ as implemented $\}$

for $r=0, \dots, k-1$ **do**

 Compute $h_{i+1/2}^{(r)}$ and $h_{i-1/2}^{(r)}$ using (A.6), and Table 3

 Compute β_r using (A.11)

 Compute α_r and $\tilde{\alpha}_r$ using Table 4 and (A.10)

end for

Compute $\sum_{s=0}^{k-1} \alpha_s$ and $\sum_{s=0}^{k-1} \tilde{\alpha}_s$

for $r=0, \dots, k-1$ **do**

 Set $\omega_r = \frac{\alpha_r}{\sum_{s=0}^{k-1} \alpha_s}$ and $\tilde{\omega}_r = \frac{\tilde{\alpha}_r}{\sum_{s=0}^{k-1} \tilde{\alpha}_s}$

end for

Construct $h_{i+1/2}^- = \sum_{r=0}^{k-1} \omega_r h_{i+1/2}^{(r)}$ and $h_{i-1/2}^+ = \sum_{r=0}^{k-1} \tilde{\omega}_r h_{i-1/2}^{(r)}$

The WENO procedure results in approximate function values at the cell edges. These values are then available for substitution into an appropriate numerical flux to compute the upwind spatial derivative, $\frac{\partial f}{\partial x}$, at the cell centers x_i . The reader may refer to relevant sections in [21] or [20], for examples of numerical flux functions.

A.3 WENO reconstruction at an arbitrary point

This section describes how the WENO procedure is adapted to reconstruct a function $f(x)$ at an arbitrary point x^* , where $x^* \in I_i$ for some $i \in \{0, 1, \dots, N-1\}$. The WENO procedure results in a degree k polynomial representation of the function $h(x)$, denoted $p(x)$, which relates to $f(x)$ as in (A.3),

$$p(x) = \sum_{j=0}^{k-1} \gamma_j x^j,$$

with the constants $\gamma_j, j=0, \dots, k-1$ determined by the WENO procedure.

The goal is to approximate the value of $f(x^*)$ using the values of $f(x)$ at the cell centers, f_i . In fact, for the approximation over the stencil $S_r(i) = \{x_{i-r}, x_{i-r+1}, \dots, x_{i-r+k-1}\}$, if $p_f(x)$ is the approximating polynomial to $f(x)$ on cell I_i , then

$$p_f^{(r)}(x^*) = \sum_{j=0}^{k-1} \hat{c}_{rj} f_{i-r+j}, \quad (\text{A.12})$$

for $r=0, \dots, k-1$. The constants \hat{c}_{rj} are computed to achieve an order k approximation to the function f . To determine the constants, let I_i be the cell in which the point x^* is located, and define (on a uniform grid)

$$\alpha = \frac{x^* - x_{i-1/2}}{\Delta x} \quad (\text{A.13})$$

so that $0 \leq \alpha < 1$ and

$$x^* = x_{i-1/2} + \alpha \Delta x. \quad (\text{A.14})$$

Given this expression, assume f is smooth in the cell I_i , expand f in a Taylor series about the point $x_{i-1/2}$ and substitute into the sum, matching terms to achieve the desired order of accuracy. The constants \hat{c}_{rj} are listed in Table 5 for $k=1, 2, 3$.

Following the above procedure results in k approximations to the value $f(x^*)$, denoted $f^{*,(r)} \equiv p_f^{(r)}(x^*)$, $r=0, \dots, k-1$. As in the above development of WENO, if the function $f(x)$ is smooth, there are constants \hat{d}_r such that

$$f^* = \sum_{r=0}^{k-1} \hat{d}_r f^{*,(r)} = f(x^*) + \mathcal{O}(\Delta x^{2k-1}). \quad (\text{A.15})$$

To find these coefficients, expand $f^{*,(r)}$ about x^* and match terms in the expansion. Consistency always results in the condition $\sum_{r=0}^{k-1} \hat{d}_r = 1$. For $k=1, 2, 3$, the constants are listed in Table 6.

Table 5: Constants for interpolation in (A.12), for $k=1,2,3$.

k	r	$j=0$	$j=1$	$j=2$
1	0	1		
2	0	$\frac{3}{2}-\alpha$	$\alpha-\frac{1}{2}$	
	1	$\frac{1}{2}-\alpha$	$\alpha+\frac{1}{2}$	
3	0	$1-\frac{(\alpha-\frac{1}{2})(\frac{7}{2}-\alpha)}{2}$	$(\alpha-\frac{1}{2})(\frac{5}{2}-\alpha)$	$\frac{(\alpha-\frac{3}{2})(\alpha-\frac{1}{2})}{2}$
	1	$1-\frac{(\alpha+\frac{1}{2})(\frac{5}{2}-\alpha)}{2}$	$(\alpha+\frac{1}{2})(\frac{3}{2}-\alpha)$	$\frac{(\alpha+\frac{1}{2})(\alpha-\frac{1}{2})}{2}$
	2	$1-\frac{(\alpha+\frac{3}{2})(\frac{3}{2}-\alpha)}{2}$	$(\alpha+\frac{3}{2})(\frac{1}{2}-\alpha)$	$\frac{(\alpha+\frac{3}{2})(\alpha+\frac{1}{2})}{2}$

Table 6: Constants \hat{d}_r from (A.15), for $k=1,2,3$.

k	d_0	d_1	d_2
1	1	-	-
2	$\frac{\alpha+\frac{1}{2}}{2}$	$\frac{\frac{3}{2}-\alpha}{2}$	-
3	$\frac{(2\alpha+3)(2\alpha+1)}{48}$	$\frac{(2\alpha+3)(5-2\alpha)}{24}$	$\frac{(2\alpha-3)(-5+2\alpha)}{48}$

The WENO procedure for approximating the value of $f(x^*)$ is obtained by applying Algorithm 1 directly to the values $f^{*,(r)}$ in place of $h_{i+1/2}^{(r)}$ and $h_{i-1/2}^{(r)}$.

References

- [1] S. Osher, L.-T. Cheng, M. Kang, H. Shim, and Y.-H. Tsai, Geometric optics in a phase-space-based level set and Eulerian framework, J. Comput. Phys., vol. 179, pp. 622–648, 2002.
- [2] K. Smith, M. Brown, and F. Tappert, Ray chaos in underwater acoustics, J. Acoust. Soc. Amer., vol. 91, pp. 1939–49, 1992.
- [3] M. Collins and W. Kuperman, Overcoming ray chaos, J. Acoust. Soc. Amer., vol. 95, pp. 3167–70, 1994.
- [4] O. Godin, Restless rays, steady wave fronts, J. Acoust. Soc. Amer., vol. 122, pp. 3353–63, 2007.
- [5] S. Osher and J. Sethian, Fronts propagating with curvature dependent speed: Algorithms based on Hamilton-Jacobi formulations, J. Comput. Phys., vol. 79, pp. 12–49, 1988.
- [6] J. Benamou, An introduction to Eulerian geometric optics (1992-2002), Jour. Sci. Comp., vol. 19, no. 1-3, pp. 63–93, 2003.
- [7] B. Engquist, O. Runborg, and A. Tornberg, High frequency wave propagation by the segment projection method, J. Comput. Phys., vol. 178, pp. 373–390, 2002.
- [8] J. Qian, L.-T. Cheng, and S. Osher, A level set-based Eulerian approach for anisotropic wave propagation, Wave Motion, vol. 37, no. 4, pp. 365–379, 2003.

- [9] L.-T. Cheng, S. Osher, M. Kang, H. Shim, and Y.-H. Tsai, Reflection in a level set framework for geometric optics, *Computer Modeling in Engineering and Sciences*, vol. 5, pp. 347–360, 2004.
- [10] B. Cockburn, J. Qian, F. Reitich, and J. Wang, An accurate spectral/discontinuous finite-element formulation of a phase-space-based level set approach to geometrical optics, *J. Comput. Phys.*, vol. 208, pp. 175–195, 2005.
- [11] J. Qian and S. Leung, A level set based Eulerian method for paraxial multivalued travel-times, *J. Comput. Phys.*, vol. 197, pp. 711–736, 2004.
- [12] J. Qian and S. Leung, A local level set method for paraxial geometrical optics, *SIAM J. Sci. Comput.*, vol. 28, no. 1, pp. 206–223, 2006.
- [13] B. Engquist and O. Runborg, Computational high frequency wave propagation, *Acta Numerica*, pp. 181–266, 2003.
- [14] M. Crandall and P.-L. Lions, Viscosity solutions of Hamilton-Jacobi equations, *Trans. Amer. Math. Soc.*, vol. 277, pp. 1–42, 1983.
- [15] J. Ogilvy, Wave scattering from rough surfaces, *Rep. Prog. Phys.*, vol. 50, no. 4, pp. 1553–1608, 1987.
- [16] F. Jensen, W. Kuperman, M. Porter, and H. Schmidt, *Computational Ocean Acoustics*. AIP Series in Modern Acoustics and Signal Processing, AIP Press, 1994.
- [17] S. Jin, H. Liu, S. Osher, and Y.-H. Tsai, Computing multivalued physical observables for the semiclassical limit of the schrödinger equation, *J. Comput. Phys.*, vol. 205, pp. 222–241, 2005.
- [18] S. Jin, H. Liu, S. Osher, and R. Tsai, Computing multi-valued physical observables for the high frequency limit of symmetric hyperbolic systems, *J. Comput. Phys.*, vol. 210, pp. 497–518, 2005.
- [19] H. Liu, S. Osher, and R. Tsai, Multi-valued solution and level set methods in computational high frequency wave propagation, *Communications in Computational Physics*, vol. 1, no. 5, pp. 765–804, 2006.
- [20] S. Osher and R. Fedkiw, *Level Set Methods and Dynamic Implicit Surfaces*, vol. 153 of Applied Mathematical Sciences. Springer, 2003.
- [21] C. Shu, Essentially non-oscillatory and weighted essentially non-oscillatory schemes for hyperbolic conservation laws, ICASE Report 97-65, NASA/CR-97-206253, November 1997.
- [22] S. Gottlieb and C. Shu, Total variation diminishing Runge-Kutta schemes, *Mathematics of Computation*, vol. 67, no. 221, pp. 73–85, 1998.
- [23] L.-T. Cheng, Efficient level set methods for constructing wavefronts in three spatial dimensions, *J. Comput. Phys.*, vol. 226, pp. 2250–2270, 2007.
- [24] M. Porter and H. Bucker, Gaussian beam tracing for computing ocean acoustic fields, *J. Acoust. Soc. Amer.*, vol. 82, pp. 1349–59, 1987.
- [25] H. Weinberg and R. Keenan, Gaussian ray bundles for modeling high-frequency propagation loss under shallow-water conditions, *J. Acoust. Soc. Amer.*, vol. 100, pp. 1421–31, 1996.
- [26] L. Kinsler, A. Frey, A. Coppens, and J. Sanders, *Fundamentals of Acoustics*. John Wiley & Sons, third ed., 1982.
- [27] T. Foreman, An exact ray theoretical formulation of the helmholtz equation, *J. Acoust. Soc. Amer.*, vol. 86, pp. 234–246, 1989.
- [28] J. Bowlin, J. Spiesberger, T. Duda, and L. Freitag, Ocean acoustical ray-tracing software RAY, Tech. Rept. WHOI-93-10, Woods Hole Oceanographic Institute, October 1992.
- [29] A. Harten, B. Engquist, S. Osher, and S. Chakravarthy, Uniformly high-order accurate essentially non-oscillatory schemes III, *J. Comput. Phys.*, vol. 71, pp. 231–303, 1987.
- [30] C. Shu and S. Osher, Efficient implementation of essentially non-oscillatory shock capturing

- schemes, *J. Comput. Phys.*, vol. 77, pp. 439–471, 1988.
- [31] C. Shu and S. Osher, Efficient implementation of essentially non-oscillatory shock capturing schemes II, *J. Comput. Phys.*, vol. 83, pp. 32–78, 1989.
 - [32] X.-D. Liu, S. Osher, and T. Chan, Weighted essentially nonoscillatory schemes, *J. Comput. Phys.*, vol. 115, pp. 200–212, 1994.
 - [33] G. Jiang and C.-W. Shu, Efficient implementation of weighted ENO schemes, *J. Comput. Phys.*, vol. 126, pp. 202–228, 1996.